Part 2: Synthesis Gas Production from Reforming of CO_2-Containing Natural Gas with Steam Using an AC Gliding Arc Discharge System: Effects of Steam Addition in Feed and Operational Parameters (submitted to *Plasma Chemistry and Plasma Processing*)

2.1 Introduction and Survey of Related Literature

In recent years, the energy demand around the world has markedly increased. As a result, many countries are aware of the shortage of fuels in the near future and have tried to encourage the use of alternative energy sources in order to reduce the demand for fossil fuels. Among the available fossil fuels, natural gas is currently considered to be an economical and substantial available resource, and it is becoming the most interesting alternative fuel for both community and industry. However, conventional natural gas reforming process (methane (CH_4) reforming) is usually operated at elevated temperatures (600–800°C), which requires an intense energy input [1]. Moreover, metal catalysts are required for the enhancement of the reaction rates, and these catalysts are seriously deactivated by the impurities in feed hydrocarbons and by carbon deposits during the reactions. Non-thermal plasma has been proposed by several studies as an alternative technique to convert natural gas to more valuable products [2-9], because of its ability to induce chemical reactions at relatively low temperatures, leading to lowering energy consumption [10]. Gliding arc discharge is one of the effective types of non-thermal plasma, and it provides the most effective non-equilibrium characteristics with simultaneous high productivity and good selectivity [11]. Therefore, gilding arc discharge was considered to be promising non-thermal plasma for reforming natural gas

in this study.

In our previous work [12,13], the challenging concept of the direct utilization of raw natural gas with a high CO_2 content was explored by using an AC low-temperature gilding arc discharge system, where the effects of each gas component in a simulated natural gas, operational parameters, and oxygen addition in feed were investigated. The results interestingly showed that the addition of a small amount of oxygen effectively minimized the carbon deposit on the electrode surface and inside the reactor wall, and also enhanced the performance of CO_2-containing natural gas reforming in terms of reactant conversion, desired product selectivity, desired product yield, and power consumption. Additionally, it was revealed that the addition of water in the form of steam to gaseous hydrocarbon feeds (e.g. methane and aliphatic hydrocarbons) improved the reaction rate, reactant conversion, product selectivity, and the ratio of hydrogen to carbon monoxide [14,15]. However, to our knowledge, the steam reforming of CO_2-containing natural gas with imitated compositions of real natural gas found in reservoirs using a gliding arc discharge system has never been investigated. Therefore, this present work aimed, for the first time, to examine the effects of hydrocarbons-to-steam molar ratio (steam content), total feed flow rate, applied voltage, and input frequency on reactant conversion, product selectivity, product yield, and power consumption for the reforming of CO_2-containing natural gas with steam using a gliding arc discharge system.

2.2 Procedure

2.2.1. Reactant Gases

The simulated natural gas used in this work consisted of CH_4, C_2H_6, C_3H_8, and CO_2, with a CH_4:C_2H_6:C_3H_8:CO_2 molar ratio of 70:5:5:20, and was specially manufactured by Thai Industry Gas (Public) Co., Ltd.

2.2.2. AC Gliding Arc Discharge System

The schematic of a low-temperature gliding arc system used in this work is shown in Figure 2.1.

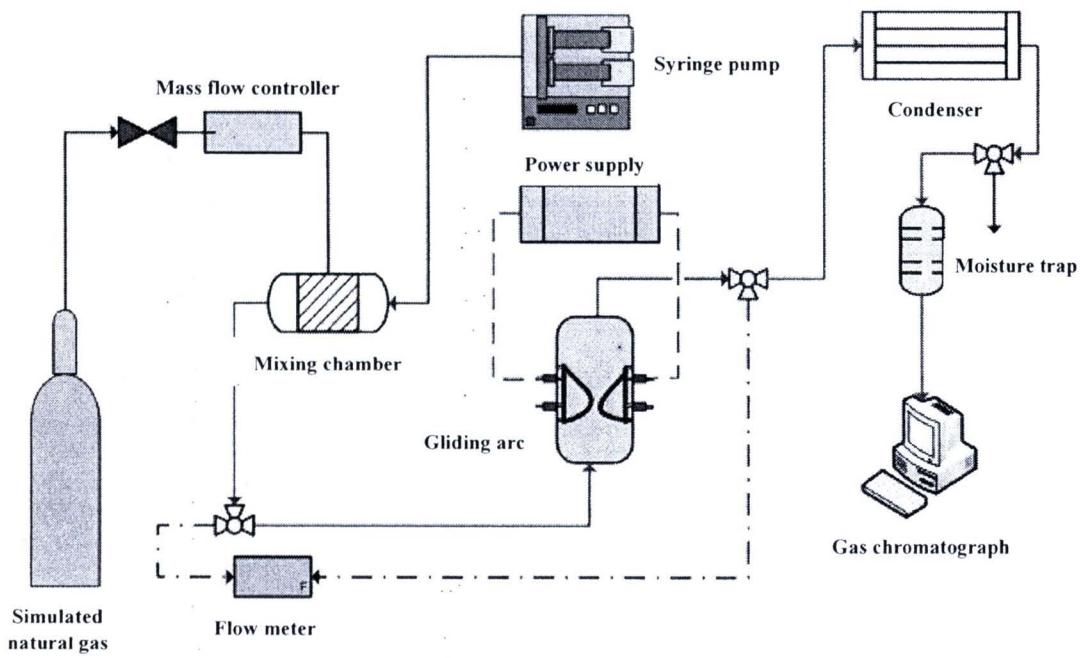

Figure 2.1 Schematic of gliding arc discharge system.

The detail of the gliding arc reactor configuration was described in our previous work [12]. A glass tube with 9 cm OD and 8.5 cm ID was used as the gliding arc reactor, which consisted of two diverging knife-shaped electrodes. The electrodes were made of stainless steel sheets with a 1.2 cm width. The gap distance between the pair of electrodes was fixed at 6 mm. The steam fed into the system was achieved by vaporizing water at a controlled temperature of 120 °C. A water flow rate was controlled by a syringe pump (Cole-Parmer). To prevent the water condensation in the feed line, the temperature of

stainless tube from the syringe pump to a mixing chamber was maintained at 120 °C by using a heating tape. The flow rate of the simulated natural gas was controlled by a mass flow controller with a transducer (AALBORG). A 7-μm stainless steel filter was placed upstream of the mass flow controller in order to trap any solid particles in the reactant gas. The check valve was also placed downstream of the mass flow controller to prevent any backflow. The reactant gas and steam were well mixed in the mixing chamber controlled at 120 °C before being introduced upward into the reactor at atmospheric pressure. The compositions of the feed gas mixture and the outlet gas were quantitatively analyzed by an on-line gas chromatograph (HP, 5890) equipped with two separate columns, i.e. a Carboxen 1000 packed column and a PLOT Al_2O_3 "s" capillary column, which were adequate to detect all hydrocarbons, CO, CO_2, and H_2.

The power supply unit consisted of three steps. For the first step, the domestic AC input of 220 V and 50 Hz was converted to a DC output of 70 V by a DC power supply converter. For the second step, a 500 W power amplifier with a function generator was used to transform the DC into AC current with a sinusoidal waveform and different frequencies. For the third step, the outlet voltage was stepped up by using a high voltage transformer. The output voltage and frequency were controlled by the function generator. The voltage and current at the low voltage side were measured instead of those at the high voltage side since the plasma generated is non-equilibrium in nature. The high side voltage and current were thereby calculated by multiplying and dividing by a factor of 130, respectively. A power analyzer was used to measure power, current, frequency, and voltage at the low voltage side of the power supply unit.

The feed gas mixture was first introduced into the gliding arc reactor without turning on the power supply unit for any studied conditions. After the compositions of

outlet gas became invariant, the power supply unit was turned on. The flow rate of the outlet gas was also measured by using a bubble flow meter. The outlet gas was analyzed by the on-line GC every 30 min. After the plasma system reached steady state with invariant outlet gas concentrations, the outlet gas was taken for analysis at least a few times every hour. The average data were used to assess the process performance of the studied gliding arc discharge system.

The plasma system performance was evaluated from reactant conversions, product selectivities, H_2 and C_2 yields, and power consumptions, as follows:

The reactant conversion is defined as:

$$\% \text{ Reactant conversion} = \frac{(\text{Moles of reactant in} - \text{Moles of reactant out}) \times (100)}{\text{Moles of reactant in}} \quad (1)$$

The selectivities of C-containing products are defined on the basis of the amount of C-containing reactants converted to any specified product, as stated in Equation 2. In the case of hydrogen product, its selectivity is calculated based on H-containing reactants converted, as stated in Equation 3:

$$\% \text{ Selectivity for any hydrocarbon product} = \frac{[P](C_P)(100)}{\Sigma[R](C_R)} \quad (2)$$

$$\% \text{ Selectivity for hydrogen} = \frac{[P](H_P)(100)}{\Sigma[R](H_R)} \quad (3)$$

where $[P]$ = moles of product in the outlet gas stream

$[R]$ = moles of each reactant in the feed stream to be converted

C_p = number of carbon atoms in a product molecule

C_R = number of carbon atom in each reactant molecule

H_p = number of hydrogen atoms in a product molecule

H_R = number of hydrogen atoms in each reactant molecule

The yields of various products are calculated using the following equations:

$$\%\ C_2 \text{ hydrocarbon yield} = \frac{[\Sigma(\%\ CH_4, \%\ C_2H_6, \%\ C_3H_8, \%\ CO_2 \text{ conversions})][\Sigma(\%\ C_2H_2, \%\ C_2H_4 \text{ selectivities})]}{(100)} \quad (4)$$

$$\%\ H_2 \text{ yield} = \frac{[\Sigma(\%\ CH_4, \%\ C_2H_6, \%\ C_3H_8 \text{ conversions})][\%\ H_2 \text{ selectivity}]}{(100)} \quad (5)$$

$$\%\ CO \text{ yield} = \frac{[\Sigma(\%\ CH_4, \%\ C_2H_6, \%\ C_3H_8, \%\ CO_2 \text{ conversions})][\%\ CO \text{ selectivity}]}{(100)} \quad (6)$$

The power consumption is calculated in a unit of Ws per C-containing reactant molecule converted and Ws per hydrogen molecule produced using the following equation:

$$\text{Power consumption} = \frac{P \times 60}{N \times M} \quad (7)$$

where P = power (W)

N = Avogadro's number (6.02×10^{23} molecule g mole^{-1})

M = rate of converted carbon in the rate of produced hydrogen molecules (g mole min^{-1})

2.3 Results and Discussion

In a plasma environment, the highly energetic electrons generated by gliding arc discharge collide with various gaseous molecules of hydrocarbons and CO_2, creating a variety of chemically active radicals. All the possibilities of chemical pathways occurring under the studied conditions are expressed below to provide a better comprehensible understanding about the plasma reforming reactions of a CO_2-containing natural gas with steam under AC non-thermal gliding arc discharge [12,13]. The radicals of oxygen active species and hydroxyl active species, as well as hydrogen, are produced during the water dissociation reactions by the collisions with electrons (Equations 8-9).

Electron-water collisions:

$$e^- + H_2O \rightarrow O^- + H_2 \quad (8)$$

$$e^- + H_2O \rightarrow OH^- + H \quad (9)$$

Additionally, the radicals of oxygen active species can be produced during the collisions of electrons on CO_2, as shown in Equations 10 and 11. Moreover, the produced CO can be further dissociated by the collisions with electrons to form coke and oxygen active species (Equation 12). The simultaneous collisions between electrons and all hydrocarbons present in the feed to produce hydrogen and various hydrocarbon species for subsequent reactions are described by Equations 13-25.

Electron-carbon dioxide collisions:

Dissociation reactions of carbon dioxide;

$$e^- + CO_2 \rightarrow CO + O^- \quad (10)$$

$$e^- + CO_2 \rightarrow CO + O + e^- \quad (11)$$

$$e^- + CO \rightarrow C + O + e^- \quad (12)$$

Electron-methane collisions:

$$e^- + CH_4 \rightarrow CH_3 + H + e^- \quad (13)$$

$$e^- + CH_3 \rightarrow CH_2 + H + e^- \quad (14)$$

$$e^- + CH_2 \rightarrow CH + H + e^- \quad (15)$$

$$e^- + CH \rightarrow C + H + e^- \quad (16)$$

$$H + H \rightarrow H_2 \quad (17)$$

Electron-ethane collisions:

$$e^- + C_2H_6 \rightarrow C_2H_5 + H + e^- \quad (18)$$

$$e^- + C_2H_5 \rightarrow C_2H_4 + H + e^- \quad (19)$$

$$e^- + C_2H_4 \rightarrow C_2H_3 + H + e^- \quad (20)$$

$$e^- + C_2H_3 \rightarrow C_2H_2 + H + e^- \quad (21)$$

$$e^- + C_2H_6 \rightarrow CH_3 + CH_3 + e^- \quad (22)$$

Electron-propane collisions:

$$e^- + C_3H_8 \rightarrow C_3H_7 + H + e^- \quad (23)$$

$$e^- + C_3H_7 \rightarrow C_3H_6 + H + e^- \quad (24)$$

$$e^- + C_3H_8 \rightarrow C_2H_5 + CH_3 + e^- \quad (25)$$

The oxygen active species derived from the CO_2 dissociation reaction can further extract hydrogen atoms from the molecules of hydrocarbon gases via the oxidative dehydrogenation reactions (Equations 26-39), consequently producing several chemically active radicals and water.

Oxidative dehydrogenation reactions:

$$CH_4 + O \rightarrow CH_3 + OH \quad (26)$$

$$C_2H_6 + O \rightarrow C_2H_5 + OH \quad (27)$$

$$C_2H_5 + O \rightarrow C_2H_4 + OH \quad (28)$$

$$C_2H_4 + O \rightarrow C_2H_3 + OH \quad (29)$$

$$C_2H_3 + O \rightarrow C_2H_2 + OH \quad (30)$$

$$C_3H_8 + O \rightarrow C_3H_7 + OH \quad (31)$$

$$C_3H_7 + O \rightarrow C_3H_6 + OH \quad (32)$$

$$CH_4 + OH \rightarrow CH_3 + H_2O \quad (33)$$

$$C_2H_6 + OH \rightarrow C_2H_5 + H_2O \quad (34)$$

$$C_2H_5 + OH \rightarrow C_2H_4 + H_2O \quad (35)$$

$$C_2H_4 + OH \rightarrow C_2H_3 + H_2O \quad (36)$$

$$C_2H_3 + OH \rightarrow C_2H_2 + H_2O \quad (37)$$

$$C_3H_8 + OH \rightarrow C_3H_7 + H_2O \quad (38)$$

$$C_3H_7 + OH \rightarrow C_3H_6 + H_2O \quad (39)$$

The C_2H_5, C_2H_3, and C_3H_7 radicals can be further converted to form ethylene, acetylene, and propane either by electron collisions (Equations 19-21, and 24) or by the oxidative dehydrogenation reactions (Equations 28-30, 32-35, 37, and 39). The extracted hydrogen atoms immediately form hydrogen gas according to Equation 17. However, no propene is detected in the outlet gas stream [13]. It is, therefore, believed that the propene species is unstable and may possibly undergo further reactions (Equations 40 and 41).

Propene hydrogenation and cracking reactions:

$$C_3H_6 + H_2 \rightarrow C_3H_8 \quad (40)$$

$$C_3H_6 \rightarrow C_2H_2 + CH_4 \quad (41)$$

In addition, the radicals of hydrocarbons and hydrogen derived from the earlier reactions further react with themselves and the other radicals to form ethane, ethylene, acetylene, propane, and butane, as shown in Equations 42-57. In addition, ethane can be further dehydrogenated to form ethylene, while ethylene can also be dehydrogenated to form acetylene by either electron collision or oxidative dehydrogenation (Equations 18, 19, 27, 28, 34, and 35 for ethylene formation; and, Equations 20, 21, 29, 30, 36, and 37 for acetylene formation).

Coupling reactions of active species:

Ethane formation reactions;

$$CH_3 + CH_3 \rightarrow C_2H_6 \quad (42)$$

$$C_2H_5 + H \rightarrow C_2H_6 \quad (43)$$

$$C_2H_5 + C_2H_5 \rightarrow C_2H_6 + C_2H_4 \quad (44)$$

$$C_3H_7 + CH_3 \rightarrow C_2H_6 + C_2H_4 \quad (45)$$

Ethylene formation reactions;

$$CH_2 + CH_2 \rightarrow C_2H_4 \quad (46)$$

$$CH_3 + CH_3 \rightarrow C_2H_4 + H_2 \quad (47)$$

$$C_2H_5 + H \rightarrow C_2H_4 + H_2 \quad (48)$$

$$C_3H_7 + H \rightarrow C_2H_4 + CH_4 \quad (49)$$

Acetylene formation reactions;

$$CH + CH \rightarrow C_2H_2 \quad (50)$$

$$CH_2 + CH_2 \rightarrow C_2H_2 + H_2 \quad (51)$$

$$CH_3 + CH \rightarrow C_2H_2 + H_2 \quad (52)$$

$$C_2H_5 + H \rightarrow C_2H_2 + H_2 + H_2 \quad (53)$$

$$C_3H_7 + H \rightarrow C_2H_2 + CH_4 + H_2 \quad (54)$$

Propane formation reactions;

$$C_2H_5 + CH_3 \rightarrow C_3H_8 \quad (55)$$

Butane formation reactions;

$$C_2H_5 + C_2H_5 \rightarrow C_4H_{10} \quad (56)$$

$$C_3H_7 + CH_3 \rightarrow C_4H_{10} \quad (57)$$

Moreover, CO can be produced under the studied conditions, particularly in feed with high oxygen content. CO may be mainly formed via the CO_2 dissociation (Equations 10 and 11). Equations 58-62 show the partial oxidative pathways of methane to form CO and H_2 as the end products. The formation of water is believed to occur via the oxidative hydrogenation reactions (Equations 33-39). In addition, water can be formed by the reactions between hydrogen or hydrogen active radical and oxygen active radical, as shown in Equations 63-65.

Carbon monoxide formation reactions:

$$CH_3 + O \rightarrow HCHO \quad (58)$$

$$HCHO + O \rightarrow OH + CHO \quad (59)$$

$$CHO + O \rightarrow OH + CO \quad (60)$$

$$CHO + OH \rightarrow CO + H_2O \quad (61)$$

$$CHO + H \rightarrow H_2 + CO \quad (62)$$

Water formation reactions:

$$2H + O \rightarrow H_2O \quad (63)$$

$$H_2 + O \rightarrow H_2O \quad (64)$$

$$H_2 + \tfrac{1}{2} O \rightarrow H_2O \quad (65)$$

Additionally, hydrocarbon molecules may crack to form carbon and hydrogen via cracking reactions (Equations 66-68).

$$CH_4 \rightarrow C + 2H_2 \quad (66)$$

$$C_2H_6 \rightarrow 2C + 3H_2 \quad (67)$$

$$C_3H_8 \rightarrow 3C + 4H_2 \quad (68)$$

2.3.1. Effect of Hydrocarbons-to-Steam Molar Ratio

The experiments were performed to initially investigate the effect of hydrocarbons-to-steam molar ratio by varying steam content in feed in the range of 0-30 mol%, while the other operating parameters were controlled at the base conditions [12]: a total feed flow rate of 100 cm^3/min, an input frequency of 300 Hz, an applied voltage of 17.5 kV, and an electrode gap distance of 6 mm. Table 1 shows the corresponding hydrocarbons-to-steam molar ratios at various steam contents used in this work.

Table 2.1 The corresponding steam contents at various hydrocarbons-to steam molar ratio

Hydrocarbons-to-steam molar ratio	Steam content (mol%)
no steam	0
9/1	10
8.5/1.5	15
8/2	20
7/3	25

The effect of steam content on reactant conversions and product yields is shown in Figure 2.2a. When the steam content increased to 10 mol%, the conversions of CH_4, C_2H_6, C_3H_8, and CO_2, as well as the H_2 yield, were remarkably enhanced as compared to the system without steam addition. Basically, in the plasma system, the steam plays an important role in providing several active species, such as OH, H, and O, from its dissociation reactions resulted from the collision by electrons (Equations 8-9). These active species can activate all reactants to form various products, leading to increasing the rates of oxidative dehydrogenation reactions and coupling reactions (Equations 26-39 and 42-57), as well as the increases in the conversions of CH_4, C_2H_6, C_3H_8, and CO_2. However, a further increase in steam content greater than 10 mol% was found to exhibit negative effects on the process performance. It should be noted that the high-energy electrons directly collide with both hydrocarbons mixture and steam, with the amount directly relative to their concentrations. As a result there are the competitive collision reactions of electrons with both hydrocarbons and steam, leading to lowering the

possibility of electron-hydrocarbon collisions at a large steam content [15]. Hence, the conversions of CH_4, C_2H_6, and CO_2, as well as the H_2 yield, decreased. Moreover, a large steam content can alter the plasma characteristics and also reduce the stability of plasma, which was directly observed from the discharge appearance and its behaviors (e.g. a smaller number of arcs produced with unsmooth arc patterns along the knife-shaped electrode pairs).

Figure 2.2b shows the outlet gas concentrations as a function of steam content. The concentrations of CH_4, C_2H_6, and CO_2 in the outlet gas tended to increase with increasing steam content from 10 to 30 mol%, corresponding to the decreases in CH_4, C_2H_6, and CO_2 conversions (Figure 2.2a). Interestingly, the concentration of C_3H_8 decreased with increasing steam content from 0-20 mol%, and increased with further increasing steam content, which corresponded well with the C_3H_8 conversion. In comparisons of all reactant conversions, the conversion was found in the following order: $C_3H_8 > C_2H_6 > CH_4 > CO_2$. These results can be explained by the differences in the bond dissociation energies of C_3H_8, C_2H_6, CH_4, and CO_2, which are 395, 410, 431, and 532 kJ/mol, respectively [12]. The higher the value of the bond dissociation energy, the lower the conversion. Thus, the C_3H_8 molecule can be much more easily converted in the plasma zone as compared to the other reactant components, even though the plasma characteristics and stability became more fluctuated at a large steam content.

Figure 2.2c shows the effect of steam content on the product selectivities. The H_2 selectivity rapidly increased with increasing steam content up to 10 mol%, and then it gradually dropped in the steam content range of 10-30 mol%. These results indicate the significant effect of the presence of steam in the plasma system, as stated above. Both the selectivities for CO and C_4H_{10} were found to slightly change with increasing steam

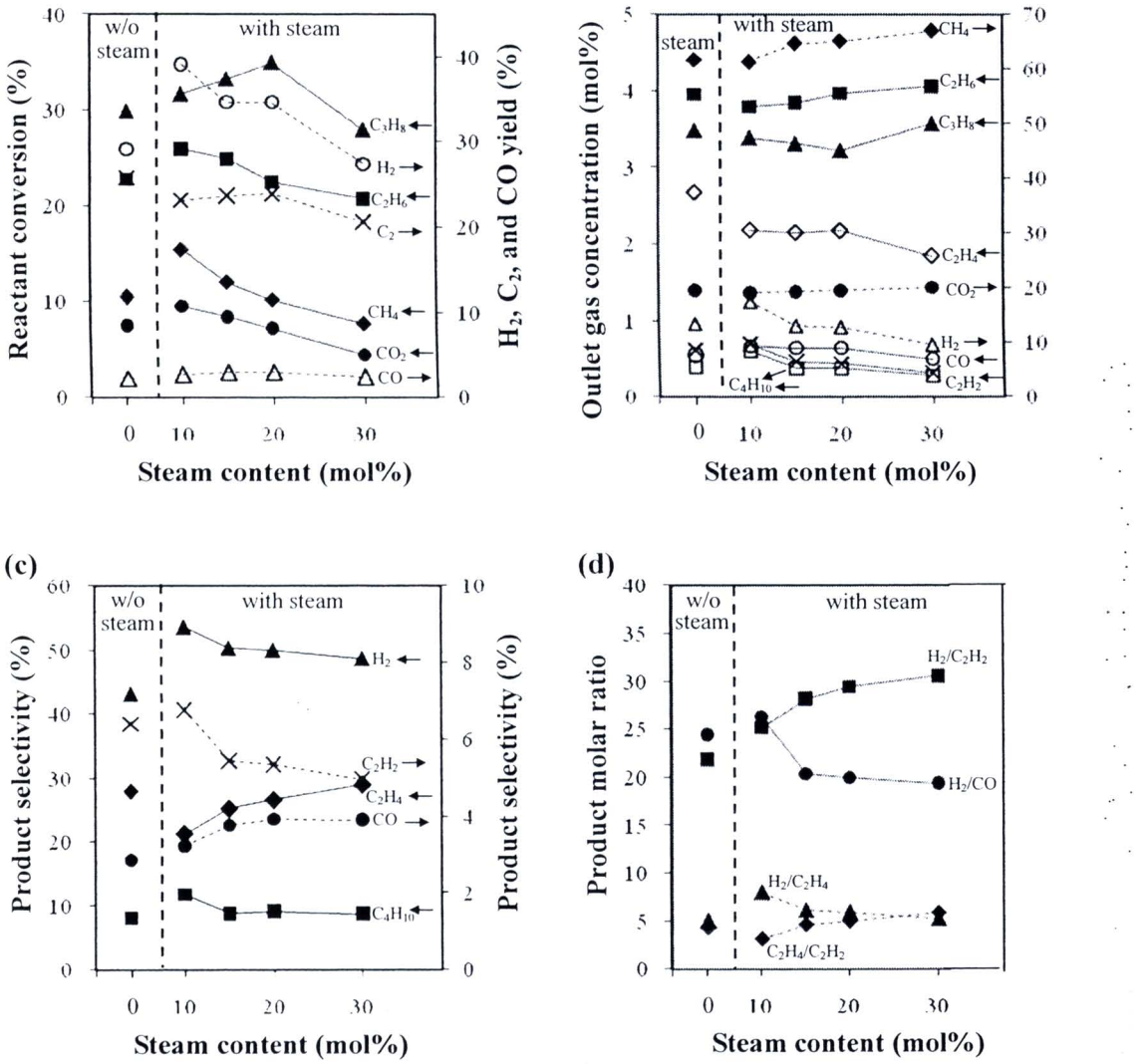

Figure 2.2 Effect of steam content on (a) reactant conversions and product yields, (b) concentrations of outlet gas, (c) product selectivities, and (d) product molar ratios for the reforming of natural gas with steam (total feed flow rate, 100 cm^3/min; applied voltage, 17.5 kV; input frequency, 300 Hz; and electrode gap distance, 6 mm).

content. The insignificant change of the CO selectivity agrees well with the CO yield, as shown in Figure 2.2a. The C_2H_2 selectivity slightly increased with increasing steam content up to 10 mol% and tended to decrease with further increasing steam content. On the other hand, the C_2H_4 selectivity showed an opposite trend. The results are well related to the molar ratios of C_2H_4/C_2H_2, H_2/C_2H_2, and H_2/C_2H_4, as shown in Figure 2.2d. The molar ratio of C_2H_4/C_2H_2 moderately decreased with increasing steam content to 10 mol%, whereas the rapid increases in both the H_2/C_2H_2 and H_2/C_2H_4 molar ratios were observed. These results indicate that the increase in H_2 production exceeds the increases in C_2H_2 and C_2H_4 production, partly due to the dehydrogenation of C_2H_4 to form H_2 and C_2H_2. It can also suggest that at the steam content of 10 mol%, the dehydrogenation of C_2H_4 is more dominant than the coupling reactions of hydrocarbon active species, leading to the consumption of C_2H_4 for a large extent to produce H_2. This possibly led to an overall decrease in the C_2 yield when increasing steam content from 0 to 10 mol % (Figure 2.2a). As mentioned above, the contradictory selectivities for C_2H_2 and C_2H_4 imply that the decrease in C_2H_4 selectivity had a more impact on the C_2 yield than the C_2H_2 selectivity in the steam content range of 0 to 10 mol%. When the steam content increased from 10 to 20 mol%, the C_2 yield remained almost unchanged (Figure 2.2a). A possible explanation is that the dehydrogenation of C_2H_4 and the coupling reactions of hydrocarbon active species simultaneously occurred at approximately the same rate. Moreover, the further increase in steam content from 20 to 30 mol% decreased the C_2 yield. It can be explained by the fact that when the steam content increased, the system had lower electrons available to collide with the reactants.

In comparisons of the H_2/CO ratios, the H_2 and CO concentrations in the outlet gas and the selectivities for H_2 and CO at different steam contents, at the steam content of

10 mol%, the system provided the highest selectivity for H_2 and the maximum molar ratios of H_2/CO and H_2/C_2H_4, suggesting the synergistic effect of steam addition on both the reactant conversions and H_2 yield, as indicated by the smoother and more stable gliding arc discharge phenomena. Therefore, the steam content of 10 mol% was preliminarily considered to be an optimum value for the reforming of CO_2-containing natural gas using gliding arc.

The effect of steam content on the power consumptions per reactant molecule converted and per H_2 molecule produced is shown in Figure 2.3. Both power consumptions first rapidly decreased with increasing steam content to 10 mol%, but dramatically increased with further increasing steam content from 10 to 30 mol%. The minimum power consumptions were about 2.12×10^{-18} Ws (13.23 eV) per reactant molecule converted and 1.95×10^{-18} Ws (12.15 eV) per H_2 molecule produced at the steam content of 10 mol%. Interestingly, it can be clearly seen that at any steam content, the power consumption per H_2 molecule produced was lower than that per reactant molecule converted, implying that the studied plasma system can be considered to be effective for producing hydrogen from the steam reforming of CO_2-containing natural gas. From the overall results, the steam content of 10 mol% was selected for further investigation.

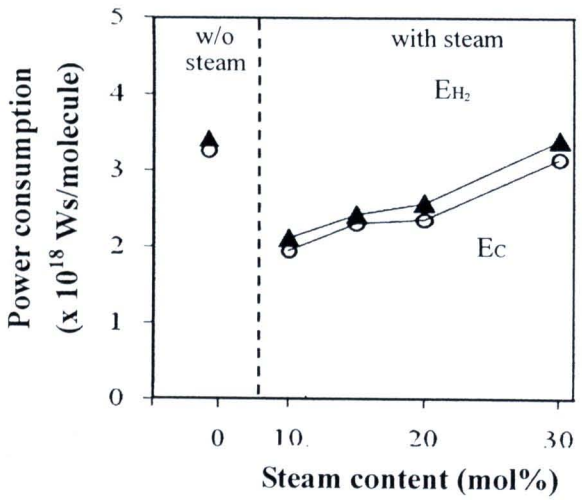

Figure 2.3 Effect of steam content on power consumptions for the reforming of natural gas with steam (total feed flow rate, 100 cm^3/min; applied voltage, 17.5 kV; input frequency, 300 Hz; and electrode gap distance, 6 mm) (E_C: power per reactant molecule converted; E_{H2}: power per H_2 molecule produced).

2.3.2. Effect of Total Feed Flow Rate and Residence Time

The effect of total feed flow rate (or residence time) on reactant conversions and product yields at a constant steam content of 10 mol% is illustrated in Figure 2.4a. The corresponding residence times at various total feed flow rates of 75, 100, 125, and 150 cm^3/min were 1.83, 1.37, 1.10, and 0.91 s, respectively. An increase in the total feed flow rate results in decreasing the residence time in the plasma reaction zone, leading to decreasing the probability of collisions between reactant molecules and highly energetic electrons. As expected, the conversions of CH_4, C_2H_6, C_3H_8, and CO_2 tended to decrease with increasing total feed flow rate or decreasing residence time. Interestingly, the H_2 yield rapidly increased with increasing total feed flow rate from 75 to 100 cm^3/min, and then sharply decreased with further increasing total feed flow rate from 100 to 150

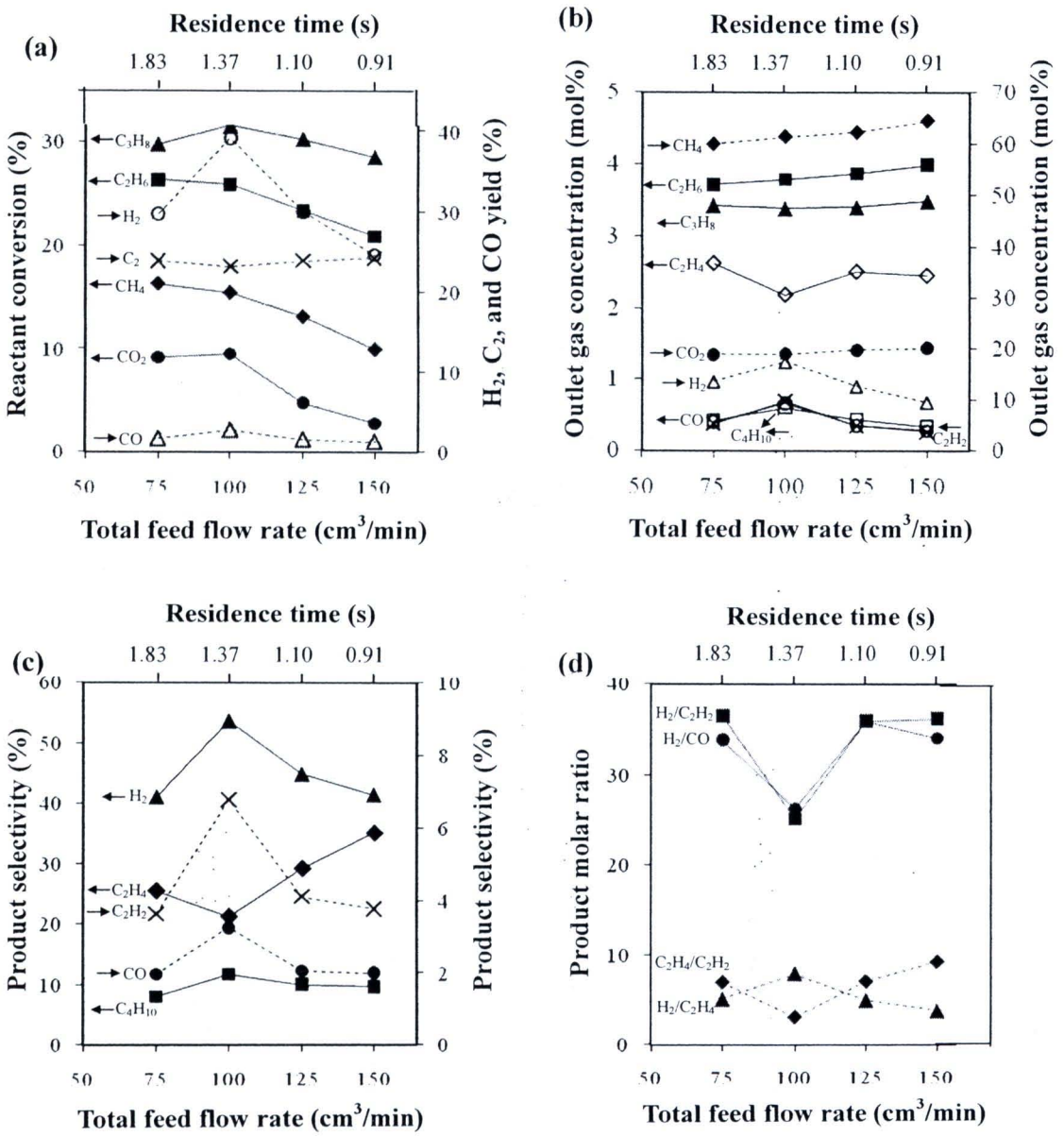

Figure 2.4 Effect of total feed flow rate on (a) reactant conversions and product yields, (b) concentrations of outlet gas, (c) product selectivities, and (d) product molar ratios for the reforming of natural gas with steam (steam content, 10 mol%; applied voltage, 17.5 kV; input frequency, 300 Hz; and electrode gap distance, 6 mm).

cm^3/min. These results well relate to the concentrations of outlet gases, particularly the H_2 concentration, as shown in Figure 2.4b. However, the increase in total feed flow rate has an insignificant impact on the C_2 and CO yields, as shown in Figure 2.4a. The concentrations of CH_4, C_2H_6, C_3H_8, and CO_2 tended to increase with increasing total feed flow rate, whereas the concentrations of H_2, CO, and C_2H_2 increased with increasing total feed flow rate from 75 to 100 cm^3/min and then decreased with further increasing total feed flow rate from 100 to 150 cm^3/min.

Figure 2.4c shows the effect of total feed flow rate or residence time on the product selectivities at a constant steam content of 10 mol%. The selectivities for H_2, CO, C_2H_2, and C_4H_{10}, initially increased with increasing total feed flow rate from 75 to 100 cm^3/min, and then sharply decreased with further increasing total feed flow rate from 100 to 150 cm^3/min. In contrast, the C_2H_4 selectivity initially decreased with increasing total feed flow rate from 75 to 100 cm^3/min and then greatly increased with further increasing total feed flow rate from 100 to 150 cm^3/min. These results also agree well with the concentrations of outlet gases, as shown in Figure 2.4b. The concentrations of H_2, CO, C_2H_2, and C_4H_{10} were found to increase with increasing total feed flow rate from 75 to 100 cm^3/min and then decreased with further increasing total feed flow rate from 100 to 150 cm^3/min. On the other hand, the concentration of C_2H_4 exhibited the opposite trend. This finding can be explained in that at a lower total feed flow rate, a greater number of energetic electrons, as well as various active species, essentially provided a comparatively higher possibility of the plasma-chemical dehydrogenation of hydrocarbon species (e.g. C_2H_4 and C_2H_6) to be converted to smaller molecules (e.g. C_2H_2, H_2, and CO), as shown in Equations 27-30, 34-37, 53, 58-62. In contrast, at a higher total feed

flow rate, the possibility of secondary dehydrogenation of hydrocarbon species decreased because of the decreasing residence time in the plasma zone. However, a further decrease in feed flow rate from 100 to 75 cm^3/min resulted in lowering all the product selectivities and the product concentrations, except C_2H_4. This result indicates that at the feed flow rate of 75 cm^3/min, the system had a very long residence time, leading to increasing the probability for the hydrogenation, or the reverse of the oxidative dehydrogenation, of C_2H_2 and the CO oxidation reaction. The maximum H_2 and C_2H_2 selectivities were observed at the total feed flow rate of 100 cm^3/min (the residence time of 1.37 s), suggesting that the dehydrogenation reaction of C_2H_4 to form C_2H_2 and H_2 preferably occurred and was maximized at this optimum total feed flow rate.

The effect of total feed flow rate on the product molar ratios is illustrated in Figure 2.4d. With increasing total feed flow rate from 75 to 100 cm^3/min, the molar ratios of H_2/CO and H_2/C_2H_2 sharply decreased, then rapidly increased with increasing total feed flow rate from 100 to 125 cm^3/min and finally remained almost unchanged with further increasing total feed flow rate from 125 to 150 cm^3/min. The molar ratio of C_2H_4/C_2H_2 slightly decreased with increasing total feed flow rate from 75 to 100 cm^3/min and then gradually increased with further increasing total feed flow rate to 150 cm^3/min. In contrast, the molar ratio of H_2/C_2H_4 slightly increased with increasing total feed flow rate from 75 to 100 cm^3/min and then decreased with further increasing total feed flow rate to 150 cm^3/min, which was in the opposite trend to the molar ratios of H_2/CO, H_2/C_2H_2, and C_2H_4/C_2H_2. These results can be correlated well with the plasma-chemical dehydrogenation behavior as stated above that the dehydrogenation reaction of C_2H_4 to form C_2H_2 and H_2, as well as the CO formation, preferably occurred at the total feed flow rate of 100 cm^3/min.

The effect of total feed flow rate on the power consumptions per reactant molecule converted and per H_2 molecule produced is shown in Figure 2.5. With increasing total feed flow rate from 75 to 100 cm^3/min, the power consumed to convert hydrogen reactant molecules and to produce hydrogen molecule significantly decreased, probably resulting from the observed good characteristic and high stability of plasma generated at the total feed flow rate of 100 cm^3/min. At a lower total feed flow rate (75 cm^3/min), the steam in the reactant feed can change the dielectric property of the system, which subsequently led to a decrease in the stability of plasma, as above mentioned. However, with further increasing total feed flow rate from 100 to 150 cm^3/min, the input power sharply increased. The increases in power consumptions at too high feed flow rates can be explained by the decreases in both reactant conversions and hydrogen production when the total feed flow rate was too high (too short residence time). Because, the minimum power consumptions were found at the total feed flow rate of 100 cm^3/min, this total feed flow rate was selected for further investigation.

2.3.3. Effect of Applied Voltage

In this present work, the effect of applied voltage was investigated by varying in the range of 12.5 to 18.5 kV. The corresponding input power at various applied voltages of 12.5, 13.5, 15.5, 17.5, and 18.5 kV were 22.1, 26.0, 26.2, 28.3, and 28.5 W, respectively, noting that the amount of input power was given from the calculation. The highest operationable applied voltage of 18.5 kV was limited by the abrupt formation of coke filament on the surfaces of the two electrodes in a relatively short operation period, which resulted in a significant decrease in the stability of plasma, while the lowest operationable applied voltage of 12.5 kV was limited by the breakdown voltage of the studied plasma system, which is a minimum voltage value required to generate a steady plasma

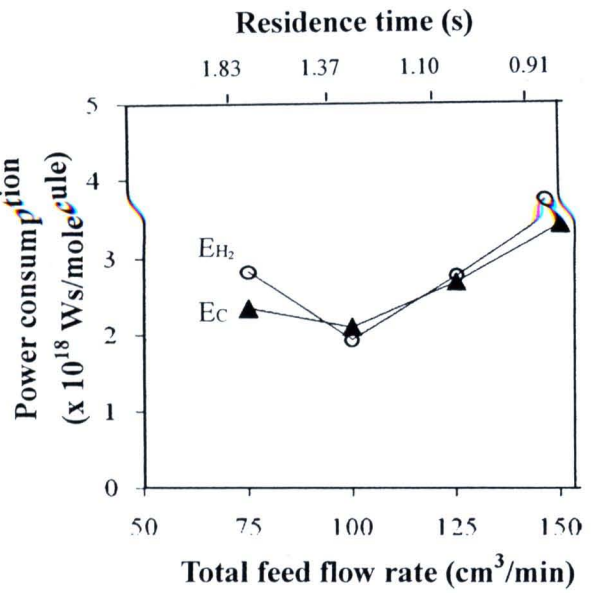

Figure 2.5 Effect of total feed flow rate on power consumptions for the reforming of natural gas with steam (steam content, 10 mol%; applied voltage, 17.5 kV; input frequency, 300 Hz; and electrode gap distance, 6 mm) (E_C: power per reactant molecule converted; E_{H2}: power per H_2 molecule produced).

discharges.

Figure 2.6a shows the effect of applied voltage on the reactant conversions and product yields at a constant steam content of 10 mol%, an input frequency of 300 Hz, and electrode gap distance of 6 mm, and a constant total feed flow rate of 100 cm^3/min. The results showed that the conversions of CH_4, C_2H_6, C_3H_8, and CO_2, as well as the H_2 and C_2 yields, tended to increase with increasing applied voltage except the CO yield remained almost unchanged. It could be clearly observed that an increase in applied voltage induces a stronger electric field strength across the electrodes, as experimentally

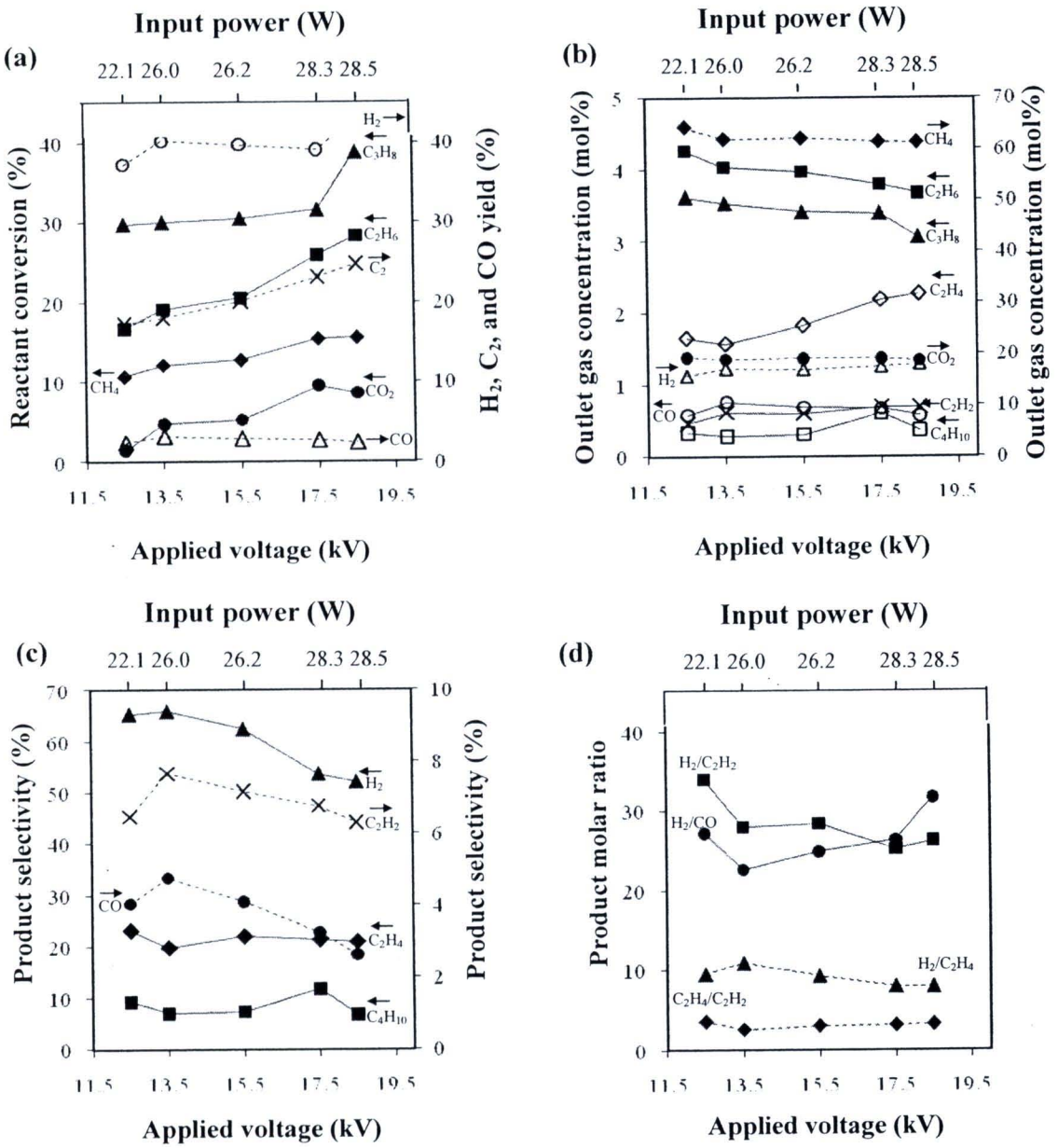

Figure 2.6 Effect of applied voltage on (a) reactant conversions and product yields, (b) concentrations of outlet gas, (c) product selectivities, and (d) product molar ratios for the reforming of natural gas with steam (steam content, 10 mol%; total feed flow rate, 100 cm^3/min; input frequency, 300 Hz; and electrode gap distance, 6 mm).

observed by an increase in input current and power. More specifically, the electric field strength is simply proportional to the mean electron energy intensity and electron temperature in the plasma [13]. Thereby, at a higher voltage, the higher input power, the generated plasma contains not only electrons with a higher average energy and temperature but also has a higher electron density. Hence, as expected, the opportunity for the occurrence of elementary chemical reactions by electron collisions (mainly ionization, excitation, and dissociation of gaseous molecules) is increased (Equations 8-25), resulting in an increase in the number of chemically active species being formed and sub-sequentially used to activate the plasma-chemical reactions [13-15, 17]. However, it was observed that the CO yield was insignificantly affected by an increase in applied voltage (Figure 2.6a). These results suggest that the partial oxidation pathways of methane to form CO and the dissociation reactions of carbon dioxide to form CO cannot complete with the other reactions.

The effect of applied voltage on the concentrations of outlet gases is illustrated in Figure 2.6b. The concentrations of CH_4, C_2H_6, C_3H_8, and CO_2 gradually decreased with increasing applied voltage, whereas the concentration of H_2 slightly increased. These results well agree with the CH_4, C_2H_6, C_3H_8, and CO_2 conversions and the H_2 yield. Figure 2.6c shows the effect of applied voltage on the product selectivities. The C_2H_2, H_2, and CO selectivities initially increased with increasing applied voltage from 12.5 to 13.5 kV and then decreased significantly with further increasing applied voltage from 13.5 to 18.5 kV. On the contrary, the selectivities for C_2H_4 and C_4H_{10} slightly decreased with increasing applied voltage from 12.5 to 13.5 kV and then tended to slightly increased with further increasing applied voltage. When considering the applied voltage range of 12.5-13.5 kV, the selectivities for C_2H_2 and H_2 increased, whereas the selectivities for

C_2H_4 and C_4H_{10} showed the opposite trends, indicating that the C_2H_2 and H_2 were preferentially produced from the dehydrogenation reactions of C_2H_4 and C_4H_{10}. A possible explanation is that at a higher applied voltage of 13.5 kV, a higher electron density, as well as a subsequent more number of active species, led to the increase in opportunity for the secondary plasma-chemical dehydrogenations of C_2H_4 and C_4H_{10}, resulting in the increase in the C_2H_2 and H_2 selectivities. However, in the applied voltage range of 13.5-18.5 kV, the decreases in the H_2 and C_2H_2 selectivities with increasing applied voltage. This is because the amount of coke deposit on the electrode surfaces was found to increase with increasing applied voltage in this studied range (7.46 % of coke at 12.5 kV, 9.15 % at 13.5 kV, 9.74 % at 15.5 kV, 10.92 % at 17.5 kV, and 13.22 % at 18.5 kV). This is possibly because at very high applied voltage, a large number of active species increased an opportunity for the secondary-dissociation reaction of CO_2 to form coke (Equation 12). In addition, the increasing tendency of the C_2H_4 and C_4H_{10} selectivities in this high applied voltage range implies that the dehydrogenation reactions are less likely to occur than the coupling reactions with increasing applied voltage.

The effect of applied voltage on the product molar ratios is shown in Figure 2.6d. The molar ratio of H_2/CO initially decreased with increasing applied voltage from 12.5 to 13.5 kV and then significantly increased with further increasing applied voltage. In the applied voltage range of 12.5-13.5 kV, the selectivity of CO rapidly increased, as mentioned above, indicating that the increase in applied voltage enhanced the dissociation reactions of CO_2 (Equations 10-11). Additionally, the result implies that, in the low applied voltage range, the CO_2 dissociation has a higher possibility to occur, as compared to the cracking of hydrocarbons to produce H_2 and coke (Equations 66-68). In the applied voltage range of 13.5-18.5 kV, the substantial increase in the molar ratio of

H_2/CO was found with increasing applied voltage because both the CO dissociation, the cracking of hydrocarbons, and the dehydrogenation reactions of hydrocarbons have higher possibilities to simultaneously occur, as compared to the CO_2 dissociation. These possible pathways are well confirmed by the observed increase in the amount of coke with increasing applied voltage. The molar ratio of H_2/C_2H_4 slightly increased with increasing applied voltage from 12.5 to 13.5 kV and then tended to decrease with further increasing applied voltage. This can be explained in that in the low applied voltage range of 12.5-13.5 kV, C_2H_4 can be selectively dehydrogenated to form H_2 via the secondary plasma-chemical dehydrogenation reaction due to the increase in the number of active species. However, at an applied voltage higher than 13.5 kV, the H_2 selectivity was found to drastically decrease (Figure 2.6c). This led to the decreases in both the molar ratios of H_2/C_2H_2 and H_2/C_2H_4 (Figure 2.6c). Interestingly, the C_2H_4/C_2H_2 molar ratio tended to slightly increase with increasing applied voltage from 13.5 to 18.5 kV (Figure 2.6d), implying that the coupling reactions preferably occur than the dehydrogenation reactions. These results were confirmed by the increase in C_2H_4 concentration (Figure 2.6b).

Figure 2.7 shows the effect of applied voltage on the power consumptions. The power consumption per reactant molecule converted (E_C) remained almost constant with increasing applied voltage from 12.5 to 13.5 kV, and it slightly increased with increasing applied voltage from 13.5 to 15.5 kV, and finally decreased with further increasing applied voltage. The decrease in power consumption per reactant molecule converted at high applied voltage range is possibly due to the rapid increase in CH_4, C_2H_6, and C_3H_8 conversions (Figure 2.6a). The power consumption per H_2 molecule produced (E_{H2})

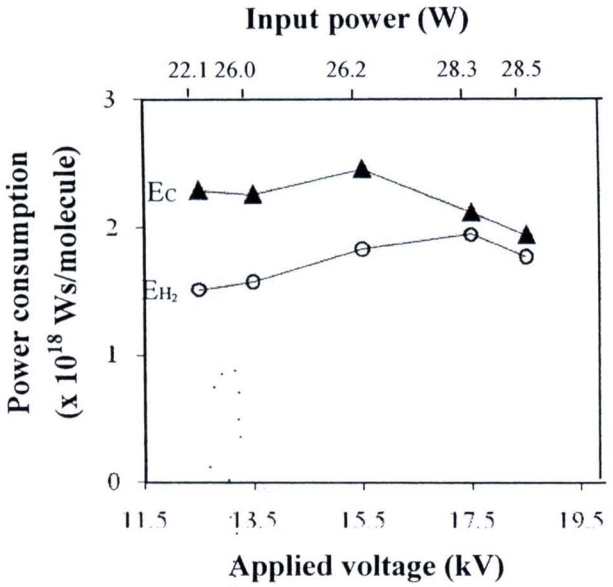

Figure 2.7 Effect of applied voltage on power consumptions for the reforming of natural gas with steam (steam content, 10 mol%; total feed flow rate, 100 cm^3/min; input frequency, 300 Hz; and electrode gap distance, 6 mm) (E_C: power per reactant molecule converted; E_{H2}: power per H_2 molecule produced).

tended to increase with increasing applied voltage from 12.5 to 17.5 kV and then decreased with further increasing applied voltage. The initial increase in the power consumption per H_2 molecule produced can be explained by the decrease in hydrogen production (Figure 2.6c). From the overall results, the optimum voltage of 13.5 kV, which reasonably provided both high selectivities for H_2 and CO and relatively low power consumptions, was selected for further experiments.

2.3.4. Effect of Input Frequency

In this present work, the input frequency was experimentally varied in the range of 300-600 Hz. The corresponding input power at various input frequencies of 300, 400,

500, and 600 Hz were 26.0, 21.7, 19.7, and 19.2 watt, respectively. The limitation of the operationable lowest frequency of 300 Hz was due to the rapid formation of coke on the electrode surfaces, leading to the interruption of the plasma generation and stability, whereas the operationable highest frequency of 600 Hz was limited by the insufficient and unstable gliding arc discharges (i.e. the extremely small number of arc produced with unsmooth arc patterns along the electrode pairs).

Figure 2.8a illustrates the effect of input frequency on the reactant conversions and product yields at a constant steam content of 10 mol%, a total feed flow rate of 100 cm^3/min, and an applied voltage of 13.5 kV, and an electrode gap distance of 6 mm. The experimental results clearly reveal that all of reactant conversions and product yields tended to decrease with increasing input frequency, corresponding to the increase in all reactant concentrations and the decrease in H_2, C_2H_2, C_2H_4, and CO concentrations in the outlet gas (Figure 2.8b). The measured current across the electrodes and input power were found to gradually decrease with increasing input frequency from 300 to 600 Hz. It is widely accepted that in an alternating current discharge system, each electrode acts alternately as an anode and cathode, due to the reversal in polarity of the electric field, and the current periodically reverse in direction. A higher frequency and a faster reversal rate in the current can cause a slower decay rate of space charges (electrons and ions) [13,17-19]. According to this reason, when employing a constant applied voltage and a fixed electrode gap distance, the current consumed to continuously activate and maintain the plasma discharge is reduced with increasing input frequency. As a result, the higher the input frequency, the lower the current, the lower the number of generated electrons and the lower the number of generated active species to initiate the plasma-chemical reactions. Based on the aforementioned phenomena relating to the input frequency, the

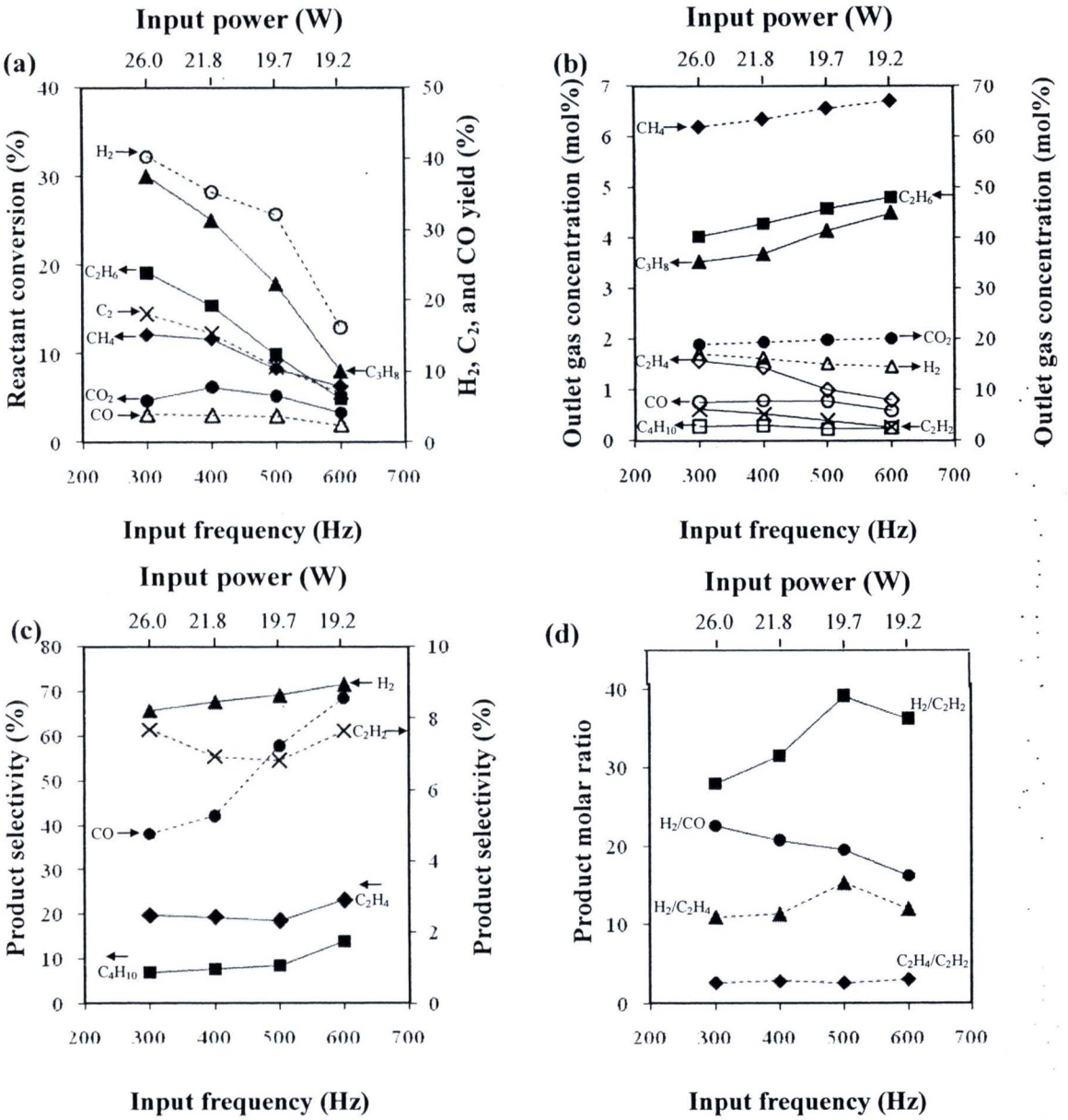

Figure 2.8 Effect of input frequency on (a) reactant conversions and product yields, (b) concentrations of outlet gas, (c) product selectivities, and (d) product molar ratios for the reforming of natural gas with steam (steam content, 10 mol%; total feed flow rate, 100 cm^3/min; applied voltage 13.5 kV; and electrode gap distance, 6 mm).

space charge characteristic of the alternating current discharge is a decisive factor that greatly influences the behaviors of discharge and the efficiency of the plasma-chemical reactions. By taking this reason into account, when the input frequency was increased, the decreases in all reactant conversions and product yields possibly resulted from the reduction of the number of generated electrons to activate the chemically active species [14,21].

The effect of input frequency on the product selectivities is shown in Figure 2.8c. With increasing input frequency, all the product selectivities except C_2H_2 tended to increase, especially the CO selectivity. However, when correlatively considering H_2, C_2H_4, and C_4H_{10} concentrations (Figure 2.8b), they slightly decreased with increasing input frequency. These results suggest that even though the reactant conversions were found to decrease, the reactants tended to be converted more selectively to H_2, CO, C_2H_4, and C_4H_{10}. For the C_2H_2 selectivity, it initially decreased with the increasing input frequency from 300 to 500 Hz and then increased with increasing input frequency from 500 to 600 Hz. The initial decrease in the C_2H_2 selectivity in the input frequency range of 300 to 500 Hz corresponded well to the decrease in the C_2H_2 concentration (Figure 2.8b). The decrease in C_2H_2 selectivity implies that the electron collisions with C_2H_4, C_2H_6, and C_3H_8 (Equations 13-24) and oxidative dehydrogenation reactions (Equations 21-39) are preferable to occur at a lower frequency (i.e. 300 Hz). For the CO concentration, it slightly increased with increasing input frequency from 300 to 500 Hz and then decreased with further increasing input frequency. These results suggest that increasing input frequency in the range of 300 to 500 Hz enabled the occurrence of carbon dioxide dissociation reactions and the oxidative dehydrogenation reactions of methane to form CO. Afterwards, at the higher input frequency range of 500-600 Hz, the number of active

species was reduced due to the undesired phenomena of space charge characteristic, as mentioned above, causing the reduction of input power. Therefore, all of the product concentrations tended to decrease.

Figure 2.8d shows the effect of input frequency on the product molar ratios. The H_2/C_2H_2 and H_2/C_2H_4 molar ratios gradually increased with increasing input frequency from 300 to 500 Hz and then rapidly decreased with further increasing input frequency. These results imply that the increase in input frequency resulted in the decreases in C_2H_2 and C_2H_4 formation rather than the decrease in H_2 formation. This led to the increase in H_2/C_2H_2 and H_2/C_2H_4 molar ratios, despite the decrease in the H_2 concentration (Figure 2.8b). With increasing input frequency, the C_2H_4/C_2H_2 molar ratio remained almost unchanged, implying that the tendency of C_2H_2 and C_2H_4 formation is in the same direction, which is consistent with the trend of H_2/C_2H_2 and H_2/C_2H_4 molar ratios. These results indicate that the oxidative dehydrogenation reactions, the electron-ethane collisions (Equations 19-21), and the coupling reactions of active species occur more preferentially at a low input frequency. For the H_2/CO molar ratio, it sharply decreased with increasing input frequency in the investigated range, probably resulted from the gradual decrease in H_2 concentration and the almost constant concentration of CO in the outlet gas stream (Figure 2.8b).

The effect of input frequency on the power consumptions is shown in Figure 2.9. It was clearly found that with increasing input frequency, both power consumptions per reactant molecule converted (E_C) and per H_2 molecule produced (E_{H2}) tended to increase. This is plausibly due to the decreases in quantities of converted reactants and of produced hydrogen when the input frequency increased. It was found that, with increasing input frequency, the intensity of the arc generated between the electrodes was reduced. This is

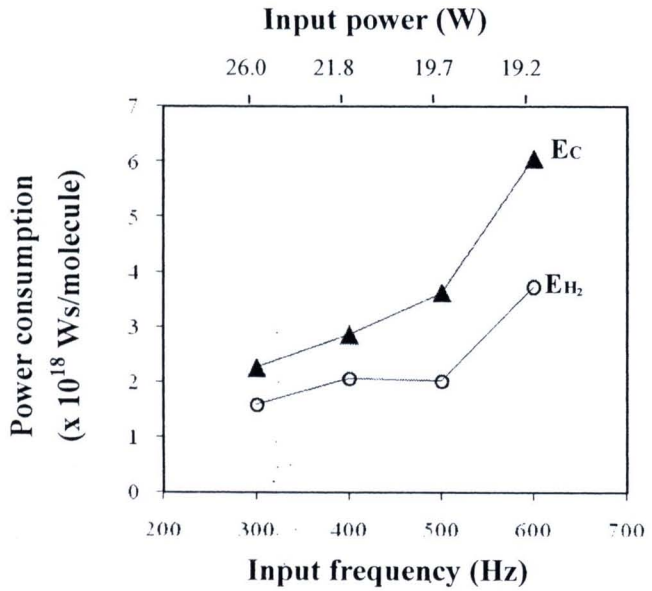

Figure 2.9 Effect of input frequency on power consumptions for the reforming of natural gas with steam (steam content, 10 mol%; total feed flow rate, 100 cm^3/min; applied voltage 13.5 kV; and electrode gap distance, 6 mm) (E_C: power per reactant molecule converted; E_{H2}: power per H_2 molecule produced).

likely because the larger number of sine-waveform cycles per second (high frequency) may require higher input energy to sufficiently sustain the gliding arc discharge, thereby reducing the intensity of the produced arc. From the overall experimental results, the operationable lowest frequency of 300 Hz was considered to be an optimum value for this investigated plasma system because it provided the highest H_2 yield, the lowest power consumptions per reactant molecule converted and per H_2 molecule produced, and the high stable plasma discharge during the system operation.

2.4 Conclusions

In this work, the reforming of CO_2-containing natural gas with steam was investigated under an AC gliding arc discharge system. The effects of hydrocarbons-to-steam molar ratio, total feed flow rate, applied voltage, and input frequency on the synthesis gas and C_2 hydrocarbon production were examined. The addition of steam content of 10 mol% to the simulated natural gas was found to greatly enhance the natural gas reforming performance in terms of reactant conversions, product yields, product selectivities, and power consumptions. All of the reactant conversions tended to increase with increasing applied voltage. However, in the applied voltage range of 13.5-18.5 kV, the decreases in both H_2 and C_2H_2 selectivities resulted from the direct observation of the rapidly increased amount of coke formed on the electrode surfaces. The increase in input frequency showed the negative effect on the reactant conversions, as well as the product yields. The optimum conditions of the investigated gliding arc discharge system were found at a hydrocarbons-to-steam molar ratio of 9/1 (a steam content of 10 mol%), a total feed flow rate of 100 cm^3/min, an applied voltage of 13.5 kV, and an input frequency of 300 Hz.

References

1. Wang B, Zhang X, Liu Y, Xu G. Conversion of CH_4, steam and O_2 to syngas and hydrocarbons via dielectric barrier discharge. J Nat Gas Chem 2009;18:94-7.

2 Sobacchi MG, Saveliev, Fridman AA, Kennedy LA, Ahmed S, Krause T. Experimental assessment of combined plasma/catalytic system for hydrogen production via partial oxidation of hydrocarbon fuels. Int J Hydrogen Energ 2002;27:635-42.

3 He JX, Han YY, Gao AH, Zhou YS, Lu ZG. Investigation on methane decomposition and the formation of C_2 hydrocarbons in DC discharge plasma by emission spectroscopy. Chin J Chem Eng 2004;12:149-51.

4 Nozaki T, Hattori A, Okazaki K. Partial oxidation of methane using a microscale non-equilibrium plasma reactor. Cataly Today 2009;98:607-16.

5 Kalra CS, Gutsol AF, Fridman AA. Gliding arc discharge as a source of intermediate plasma for methane partial oxidation. IEEE Trans Plasma Sci 2005;33:32-4.

6 Paulmier T, Fulcheri L. Use of non-thermal plasma for hydrocarbons reforming. Chem Eng J 2005;106:59-71.

7 Wang Y, Liu CJ, Zhang YP. Plasma methane conversion in the presence of dimethyl ether using dielectric-barrier discharge. Energ & Fuel 2005;19:877-81.

8 Ahmar E El, Met C, Aubry O, Khacef A, Cormier JM. Hydrogen enrichment of a methane-air mixture by atmospheric pressure plasma for vehicle applications. Chem Eng J 2009;116:13-8.

9 Bromberg L, Cohn DR, Rabinovich A, Alexeev N, Samokhin A, Hadidi K, et al. Onboard plasmatron hydrogen production for improved vehicles. MIT Plasma Sci & Fus Cent 2006;JA-06-3:1-173.

10 Petitpas G, Rollier JD, Darmon A, Gonzalez-Aguilar J, Matkemeijer R, Fulcheri L. A comparative study of non-thermal plasma assisted reforming technologies. Int J Hydrogen Energ 2007;32:2848-67.

11 Fridman A, Kennedy LA. Plasma Physics and Engineering. Taylor & Francis. New York; 2004.

12 Rueangjitt N, Akarawitoo C, Sreethawong T, Chavadej S. Reforming of CO_2-containing natural gas using an AC gliding arc system: Effect of gas component in natural gas. Plasma Chem Plasma Process 2007;27:559-76.

13 Rueangjitt N, Sreethawong T, Chavadej S. Reforming of CO_2-containing natural gas using an AC gliding arc system: effects of operational parameters and oxygen addition in feed. Plasma Chem Plasma Process 2008;28:49-67.

14 Supat K, Chavadej S, Lobban LL, Millinson GR. Combined steam reforming and partial oxidation of methane to synthesis gas under electrical discharge. Ind & Eng Chem Res 2003;42:1654-61.

15 Sugasawa M, Terasawa T, Futamura S. Effects of initial water content on steam reforming of aliphatic hydrocarbons with nonthermal plasma. J Electrostat 2010;68:212-7.

16 Dean JA. Lange's Handbook of Chemistry. McGraw-Hill. New York; 1999.

17 Sreethawong T, Thakonpatthanakun P, Chavadej S. Partial oxidation of methane with air for synthesis gas production in a multistage gliding arc discharge system. Int J Hydrogen Energ 2007;32:1067-79.

18 Zielinski T, Kijenski J. Plasma carbon black the new active additive for plastic. Composit Part A : Appl Sci Manufact 2005;36:467-71.

19 Opalinska T, Zielinski T, Schmidt-Szalowski K. Carbon black generation in gliding arc discharges. Polish J Chem 2003;77:1357-61.

20 Supat K, Kruapong A, Chavadej S, Lobban LL, Millinson GR, Mallinson RG. Synthesis gas production from partial oxidation of methane with air in AC electric gas discharge. Energ & Fuel 2003;17:471-81.